Experimental constraints on the ordinary chondrite shock darkening caused by asteroid collisions

Tomas Kohout[1], Evgeniya Petrova[2], Grigoriy Yakovlev[2], Victor Grokhovsky[2], Antti Penttilä[1],Alessandro Maturilli[3], Juulia-Gabrielle Moreau[1], Stepan Berzin[4], Joonas Wasiljeff[1], Dmitry Zamyatin[2,4], Razilia Muftakhetdinova[2], and Mikko Heikkilä[1]

1. University of Helsinki, Faculty of Science, Helsinki, Finland (tomas.kohout@helsinki.fi)
2. Institute of Physics and Technology, Ural Federal University, Ekaterinburg, Russian Federation
3. Institute of Planetary Research, DLR, Berlin, Germany
4. Zavaritsky Institute of Geology and Geochemistry, Ural Branch of the Russian Academy of Sciences, Ekaterinburg, RussianFederation

Introduction

Shock-induced changes in planetary materials related to impacts or planetary collisions are known to be capable of altering their optical properties. One such example is observed in ordinary chondrite meteorites. The highly shocked silicate-rich ordinary chondrite material is optically darkened and its typical S-complex-like asteroid spectrum is altered toward a darker, featureless spectrum resembling the C/X complex asteroids. Thus, one can hypothesize that a significant portion of the ordinary chondrite material may be hidden within the observed C/X asteroid population.

The exact pressure-temperature conditions of the shock-induced darkening are, however, not well constrained and due to this gap in knowledge, it is not possible to correctly assess the significance of the shock darkening within the asteroid population. In order to address this shortcoming, we experimentally investigate the gradual changes in the chondrite material optical properties together with the associated mineral and textural features as a function of the shock pressure. For this purpose, we use a Chelyabinsk meteorite (LL5 chondrite), which is subjected to a spherical shock experiment. The spherical shock experiment geometry allows for a gradual increase in the shock pressure within a single spherically shaped sample from 15 GPa at its rim toward hundreds of gigapascals in the center.

Results

Four distinct zones were observed with an increasing shock load (Fig. 1). We number the zones in the direction of increasing shock from the outside toward the center as zones I–IV The optical changes in zone I are minimal up to ~50 GPa. In the region of ~50–60 GPa corresponding to zone II, shock darkening occurs due to the troilite melt infusion into silicates. This process abruptly ceases at pressures of ~60 GPa in zone III due to an onset of silicate melting and immiscibility of troilite and silicate melts. Silicate melt coats residual silicate grains and prevents troilite from further penetration into cracks. At pressures higher than ~150 GPa (zone IV), complete recrystallization occurs and is associated with a second-stage shock darkening due to fine troilite-metal eutectic grains. The order of the spectral curves in the UV-VIS-NIR (ultraviolet – visible – near-infrared) region follows the visual brightness in which zone I is the brightest, followed by zones III and II, and zone IV is the darkest one (Fig. 2). The MIR reflectance (Fig. 3) follows the same albedo order as UV-VIS-NIR up to the primary Christiansen feature at 8.7 µm. At higher wavelengths in the Si-O reststrahlen bands region, the reflectance order changes with zones II and III, which are

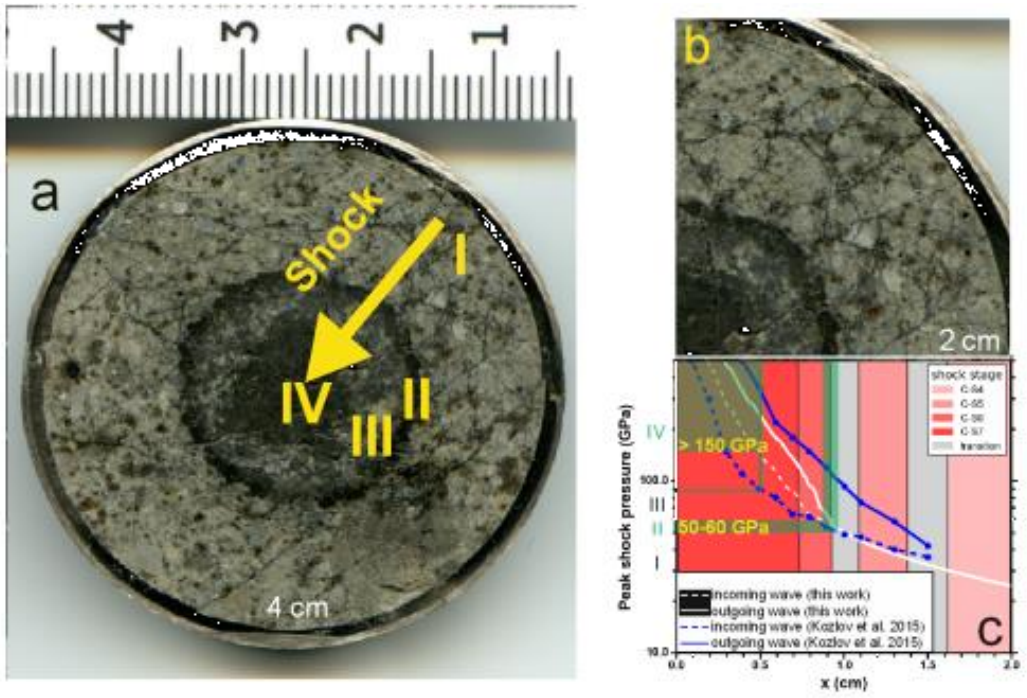

Fig. 1. a: spherically shocked Chelyabinsk meteorite sample. The arrow outlines the direction of increasing shock. The roman numbers distinguish the four different shock zones. b and s: comparison of the experiment result (b, zoomed upper-right quadrant of a) to the iSALE modeling results of the spherical shock experiment (c) with the shock stage intervals. The green areas in (c) outline the location of the shock-darkened zones II and IV, together with their pressure boundaries calculated from the inward shock wave peak shock pressures from our iSALE model.

brighter than zones I and IV. The comparison of the powdered sample spectra to the one obtained from the rough saw-cut surface reveals the following trends. The overall reflectance of the powdered sample is an order of magnitude lower compared to the rough surface one. The reststrahlen bands in both samples show similar positions at approximately 9.1, 9.5–9.6, 10.3, 10.8, 11.3, and 11.8–12 µm. They are dominated by olivine with possible presence of orthopyroxene. The amplitudes of the reststrahlen bands are higher in the rough surface sample. The transparency feature at 12.7 µm is only observed in the powdered sample. The primary Christiansen feature at 8.7 µm is more pronounced in the powdered sample, while the secondary one at 15.6 µm is of a low amplitude in both samples.

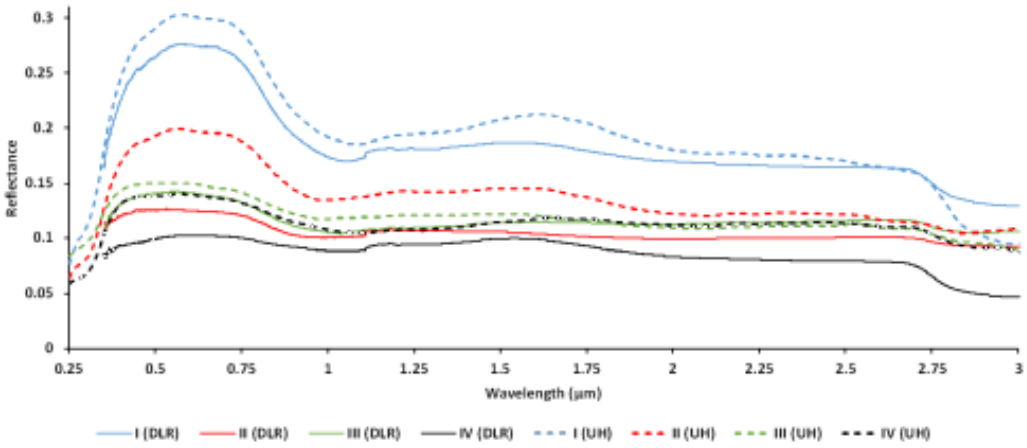

Fig. 2. Comparison of the UV-VIS-NIR bidirectional (measured at DLR) and hemispherical (measured at UH) reflectance.

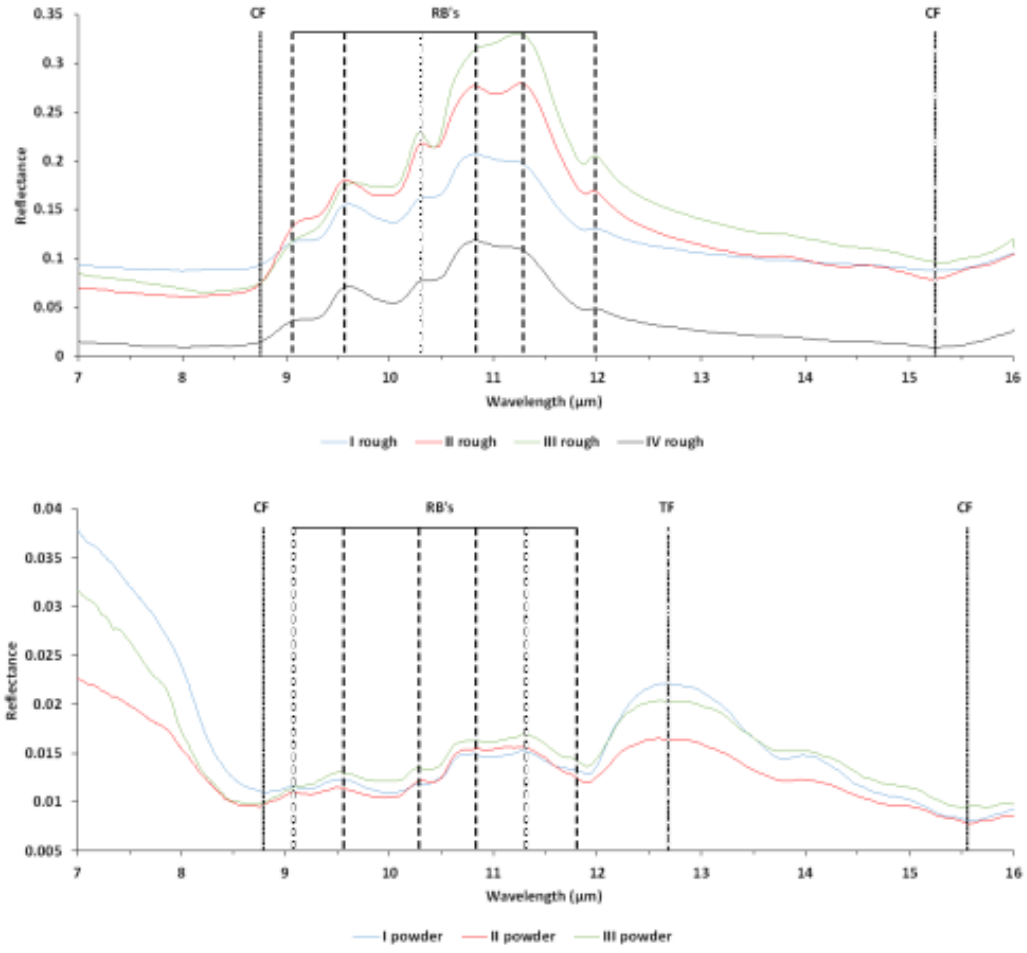

Fig. 3. Comparison of the MIR bidirectional (DLR) reflectance of the four zones measured on a saw-cut surface (top) and powder (bottom). CF,RB, and TF stand for the Christiansen feature, reststrahlen bands, and the transparency feature, respectively.

Conclusions

The important finding is the presence of the two distinct shock darkening mechanisms in ordinary chondrite material with characteristic material fabric and distinct pressure regions. These two regions are separated by a pressure interval where no darkening occurs. Thus, the volume of the darkened material produced during asteroid collisions may be somewhat lower than assumed from a continuous darkening process. While the darkening mainly affects the UV-VIS-NIR region and 1 and 2-µm silicate absorption bands, it does not significantly affect the silicate spectral features in the MIR region. These are more affected by material roughness. MIR observations have the potential to identify darkened ordinary chondrite material with an otherwise featureless UV-VIS-NIR spectrum.

Reference: Kohout T., et al. (2020): Experimental constraints on the ordinary chondrite shock darkening caused by asteroid collisions. Astronomy & Astrophysics, 639, A146. https://doi.org/10.1051/0004-6361/202037593

Full resolution images and raw data: https://dx.doi.org/10.5281/zenodo.3584942